Full Paper

Isolation and profiling of circulating tumor-associated exosomes using extracellular vesicular lipid-protein binding affinity based Microfluidic device

Yoon-Tae Kang[1], Emma Purcell[1], Colin Palacios-Rolston[1], Ting-Wen Lo[1], Nithya Ramnath[2], Shruti Jolly[3] and Sunitha Nagrath[1]

[1]Dr. Yoon-Tae Kang, Emma Purcell, Colin Palacios-Rolston, Ting-Wen Lo, Prof. Sunitha Nagrath
Department of Chemical Engineering and Biointerface Institute, University of Michigan, 2800 Plymouth Road, NCRC B10-A184, Ann Arbor, MI 48109, USA
E-mail: snagrath@umich.edu

[2]Dr. Nithya Ramnath
Department of Internal Medicine, University of Michigan, Ann Arbor, MI 48109, USA

[3]Dr. Shruti Jolly
Radiation of Oncology, University of Hospital, University of Michigan, 1500 E Medical Center Dr. Ann Arbor, MI 48109, USA

Extracellular vesicles (EV) are emerging as a potential diagnostic test for cancer. Owing to the recent advances in microfluidics, on-chip EV isolation are showing promise with respect to improved recovery rates, smaller necessary sample volumes, and shorter processing times than an ultracentrifugation. Immunoaffinity-based microfluidic EV isolation using anti-CD63

has been widely used, however, anti-CD63 is not specific to cancer-EVs, and some cancers secrete EVs with low expression of CD63. Alternatively, phosphatidylserine (PS), usually expressed in the inner leaflet of the lipid bilayer of the cells, has been shown to be expressed on the outer surface of cancer-associated EVs. We present a new exosome isolation microfluidic device (^{new}ExoChip), conjugated with PS-specific protein, to isolate cancer-associated exosomes from plasma. Our device achieves 90% capture efficiency for cancer cell exosomes compared to 38% for healthy exosomes and isolates 35% more A549-derived exosomes than an anti-CD63-conjugated device. Immobilized exosomes are then easily released using Ca^{2+} chelation. The recovered exosomes from clinical samples were characterized by electron microscopy and western-blot analysis, revealing exosomal shapes and exosomal protein expressions. The ^{new}ExoChip facilitates the isolation of a specific subset of exosomes, allowing us to explore the undiscovered roles of exosomes in cancer progression and metastasis.

1. Introduction

The liquid biopsy has emerged as a diagnostic and prognostic tool in cancer, overcoming many of the drawbacks associated with conventional tissue-biopsy based methods. Several biomarkers in the blood, such as circulating tumor cells (CTCs) and cell-free nucleic acids (cfNAs), are finding use in the laboratory and in the clinic to guide important clinical decisions regarding cancer diagnosis and therapies. These circulating markers also give us a window to study cancer biology, including dissemination and metastasis, and may eventually assist in the clinical setting by identifying patient's potential for metastasis after surgery for early stages of cancer.

Exosomes, secreted by various cells and released into extracellular environments, are nanometer sized vesicles conformed by a phospholipid bilayer. Recent studies showed that exosomes contain a number of proteins and nucleic acids allowing them to function as vesicular messengers between cells. Cell to cell communication was previously thought to be possible only by several well-known signaling methods including endocrine, paracrine, and juxtacrine (contact-dependent) signaling. The role of exosome-mediated intercellular communication is quickly gaining interest. Studies have highlighted that exosome mediated cell-cell communication may play a critical role in disease progression by facilitating the cell involvement in this process.[1-3] Similarly, research reveals that tumor cell-derived exosome or tumor microenvironment-derived exosome can spread into extracellular environments and promote cancer progression and metastasis.[4-6] Therefore, it is both relevant and necessary to further study how these cancer-associated exosome could contribute to the diagnostic potential provided by the liquid biopsy tool. In order to use these exosomes as diagnostic markers, highly purified cancer-associated exosome isolation, characterization and validation methods are essential. [7]

Ultracentrifugation (UC) has thus far been the gold standard for the isolation of these cancer-associated exosomes for biological research. However, this method suffers from drawbacks such as lengthy processing time, low recovery rates and an inability to handle small sample volumes [8]; these drawbacks are offset by ease of use and minimal need for technical expertise. Several groups have reported on the potential and clinical significance of these exosomes.[9,10] For example, Marta et al. used ultracentrifugation to isolate exosomes from ovarian cancer patients and showed that plasma from ovarian cancer patients contained higher levels of exosomal proteins compared to those from benign tumor patients or healthy

controls. [9] Recently, An et al isolated exosomes from pancreatic cancer patients and were able to demonstrate the role of these exosomes in inducing cell migration in *ex-vivo* experiments, supporting the idea that exosomes may be involved in metastasis.[10] However, UC based isolation methods are unable to distinguish exosomes from other extracellular vesicles or large protein debris having similar density. Additionally, the need for many washing and handling steps during UC inevitably cause a high degree of sample loss, which is a distinct disadvantage for samples with a low starting number of exosomes. Recently, polymer-based exosome isolation kits have been developed and are available in the market. These kits use comparably low-speed centrifugation for exosome isolation with the help of polymer-assisted nanoparticle precipitation in liquid phase. Although their inclusive sedimentation of vesicles is helpful for downstream analysis, there is loss of specificity, which makes quantitative analysis of exosomes difficult.

Microfluidics technologies offer many advantages and may become the optimal method for exosome isolation in the future. Owing to recent advances in microfluidic technologies, several microfluidic devices for exosome isolation have been developed with better recovery and shorter processing times compared to UC. [11-17] Among them, immunoaffinity-based microfluidic isolation using antibodies against exosomal surface proteins is advantageous as it allows for high specificity exosome isolation from heterogeneous samples, such as plasma, serum, or urine. This method also has been incorporated with an engineered surface or characteristic patterns in order to enhance the efficiency of exosome isolation. [11, 12, 14] As an example, antibodies against the tetraspanin CD63 have been widely applied to exosome isolation from the plasma of patients with ovarian cancer, breast cancer, and glioblastoma. [12, 14, 18-21] However, anti-CD63 is not a specific biomarker for any one cancer, and its expression

is known to vary depending on the type of cancer. [22] Recent studies using clinical samples showed that only 69.56% of lung cancer patients have CD63 positive exosomes with comparably low absolute expression level compared to other exosomal markers. [23, 24] To date, a few cancer-specific exosomal proteins such as EGFR, PSA, and HER2 have been incorporated into microfluidics for cancer-associated exosome isolation for lung, prostate, and breast cancers respectively.[25-27]

In addition to targeting exosomal surface proteins, alternative approaches to target certain types of exosomal lipids have been studied by a few groups. Mass spectrometry has revealed a 2-3 fold greater enrichment of cholesterol, sphingomyelin (SM), glycosphingolipids, and phosphatidylserine (PS) in exosomes compared to cells. [28]

Among the lipids, phosphatidylserine (PS) is a type of phospholipid that lies within the inner leaflet of the normal cell membrane but becomes externalized in malignant and apoptotic cells. Because exposed PS typically functions as an 'eat me' signal for macrophages in our immune system, these cells or vesicles with PS are generally removed from circulation. Recent studies have revealed that PS is externalized not only on apoptotic cells but also on microvesicles and exosomes during vesiculation. [29-32] A few studies have also reported that PS expression on the membrane leaflet is more abundant in cancer cells [33] and cancer cell derived exosomes [34] compared to those from healthy controls. In order to detect and quantify the PS expression on cells or vesicle surfaces, several proteins have been tested and specific binding affinities of Tim4 [35] and annexin V [36] to PS have been proved. One of the most widely studied PS-binding molecules, annexin V, is a 35.8kDa protein which binds PS in a calcium dependent manner. [37] Given that PS expression on cancer cells and cancer cell-derived exosomes is higher than those of normal cell and normal cell-derived exosomes, one

can posit that cancer-derived exosomes can be isolated using an annexin V-immobilized microfluidic device, and the isolated specific exosome can be released by Ca^{2+} chelation. Moreover, this lipid-based isolation is more likely to enrich the purified exosomes regardless of their CD63 expression, making it feasible to isolate the cancer exosomes from CD63-downregulated cancers, such as lung cancer. Recently, there have been attempts to isolate cancer derived exosomes using their characteristic lipid expression. [35, 38] Wataru et al. used T-cell immunoglobulin mucin protein 4 (Tim-4) to isolate extracellular vesicles. They immobilized Tim4 on conventional magnetic beads and applied them to cell culture supernatant with hematopoietic and cancer cells. Their results from extensive downstream analysis of isolated exosomes showed PS-based extracellular vesicle isolation is feasible. They did not, however, demonstrate the feasibility of the release of these extracellular vesicles from a microfluidic device for further downstream applications. Similar to Wataru's work, Huiying et al. used Tim4 beads to purify extracellular vesicles before the quantitative detection of CD63-positive exosomes. Using 10 serum samples from patients with hepatocellular cancer, they showed that PS-based purification of exosomes allowed for the distinguishing of cancer patients from healthy donors.[38] However, they still used CD63 for exosome confirmation, therefore this platform may not be applicable to patients whose cancers present downregulated CD63. To the best of our knowledge, there are no known studies that report on lipid-affinity based microfluidic exosome isolation and their clinical applications.

Our group previously presented the ExoChip which isolates exosomes using microfluidic devices using anti-CD63-exosome affinity.[11] Its novel design and significance revealed that exosomes can be efficiently isolated from the serum samples, and that their downstream

analysis might give us clues regarding their role in cancer biology. However, due to the lack of releasing mechanism of the captured exosomes, qualitative analysis and functional studies of exosomes have been limited. Taking into consideration the greater merits of lipid-affinity-based exosome isolation, we present a newer version of our exosome isolation microfluidic device, [new]ExoChip. The annexin V immobilized microfluidic is designed with alternating narrow and wide ripple-like design inspired by the ExoChip that enhances the binding interaction between specific exosomes and PS-targeting molecules, thus resulting in higher capture efficiency and purity at conditions of high flow rates (**Figure 1**). Compared to our previous ExoChip, the [new]ExoChip having 225 times more micro-sized circular chambers, enabling faster sample processing with higher selectivity (Table S1). We extended our study to clinical blood samples from patients with non-small cell lung cancer (NSCLC) and melanoma in order to verify the translational potential of our devices. Liquid biopsy studies in lung cancer have mostly been limited to CTCs and ctDNA, many of which still require clinical validation as diagnostic and prognostic markers. More recently these studies have included cancer exosomes, where groups have described important correlations between tumor progression and exosome numbers. Patients with lung adenocarcinoma presented with higher numbers of exosomes in the blood compared with healthy controls.[39] Accumulating evidence suggests that exosomal cargos in lung cancer serves as a potential biomarker for diagnosis and prognosis. However, due to limitations pertaining to sensitivity of the technologies, comprehensive studies are lacking. Similarly, in another aggressive cancer, malignant melanoma, there have been few studies that have reported that conventional exosome isolation methods may not be useful in distinguishing cancer from healthy controls due to limited number of melanoma-associated exosomes that are shed into the blood. [40] Therefore, we have focused our efforts in studying our new device in these two cancers.

2. Results and discussion

2.1. Evaluation of binding affinity between ^{new}ExoChip device and cancer exosomes

For the initial performance evaluation of the microfluidic exosome isolation, we used two quantitative analysis methods: **1)**DiO lipophilic dye staining and **2)**Scanning electron microscope (SEM). The DiO staining, which is specific to the lipid bilayer that encompasses extracellular vesicles, is beneficial for simple confirmation of exosome isolation using conventional fluorescence microscopy. DiO staining showed greater fluorescence intensity on the ^{new}ExoChip compared to devices that had not been functionalized and devices with no antibody (**Figure 2**). These results demonstrate that the present device is capable of capturing vesicles via specific interaction through annexin V and not by non-specific binding. From preliminary studies using small chamber devices and PDMS blocks (Supporting Information **S5**), we confirmed that annexin V captured more exosomes compared to an anti-CD63 based immuno-affinity method. As such, we have demonstrated that when used with microfluidics, annexin V-conjugated devices are able to capture and release high numbers of exosome-like vesicles.

The SEM analysis gave us more detailed capture quantification and size information about the exosomes captured on our device. SEM results verified successful isolation, and the subsequent release, of particles using the ^{new}ExoChip functionalized with annexin V. A control sample was run using a device without annexin V conjugation and shows negligible non-specific binding of exosomes. Microscope images of the devices after release showed a lower concentration of exosomal particles attached to the device as compared to the samples

where no release was performed. From SEM images, the sizes of captured exosomes are in the range of exosome sizes reported by previous studies. [41-43] This data verified that the newExoChip, when functionalized with annexin V, is capable of both selectively capturing exosomes where a non-functionalized device could not and releasing a considerable number of exosomes after calcium chelation using EDTA.

2. 2. Optimization of the newExoChip devices and sample processing conditions

The device has been optimized with respect to optimal concentration of reagents, sample volume, and processing flow rates. This optimization was evaluated in terms of capture efficiency, release efficiency, specificity, and recovery rate. The definitions of those terminologies are summarized in Supporting Information **S6**. In brief, capture efficiency is the fraction of the isolated exosome-sized vesicles by the device compared to initial number of spiked exosome in the initial sample. Release efficiency is the fraction of the released exosomes from the device using calcium chelating agent compared to the number of the isolated exosomes. Specificity is the fraction of exosome sized vesicles compared to the whole concentration of vesicles. Recovery rate is another term for more heterogeneous samples, such as plasma and cell culture supernatant. This term is defined as the fraction of exosomes released from the device compared to sum of exosome sized vesicles in capture effluent and release resultant. For calculating the aforementioned evaluation criteria in quantitative way, we used Nanoparticle Tracking Analysis (NTA) on Malvern's NanoSight and evaluated size distribution and exosomal concentration of samples.

First, the annexin V concentration for device conjugation was optimized. Three different amounts of biotinylated annexin V were evaluated in terms of spiked exosome capturing efficiency. NTA analysis shows higher capture efficiency of A549 derived exosomes when the device was conjugated with over 600ng (10μl) of biotinylated annexin V as opposed to the device with 300ng (5μl) (**Figure 3**a). Even though 900ng (15μl) showed slightly higher capture efficiency of A549 exosomes, the difference between 600ng and 900ng was insignificant. As such, we immobilized the biotinylated-annexin V with a dilution ratio of 1:10 (600ng) for all subsequent experiments. In order to determine the optimal concentration of EDTA for Ca^{2+} chelation and subsequent exosome release, four different EDTA concentrations were applied to the device after capture. Theoretically, using the same molar concentration of EDTA in the release solution to that of Ca^{2+} in the binding buffer solution (2.5mM) is enough for full chelation of calcium between the device surface and exosomes. However, we found that a higher EDTA concentration, up to 20mM, worked well in our system. Release efficiency rose steadily with increasing EDTA concentration, reaching peak efficiency at 20mM and dropping at 40mM (**Figure 3**b). Therefore, 20mM was decided as the optimal concentration. Recent studies showed that high concentrations of EDTA solution may affect vesicle fusion or aggregation by promoting fluidization and destabilization of membranes.[44, 45] Our NTA size distribution results were also in accordance with these results, showing aggregated particles sizing over 200μm at high EDTA concentrations (**Figure S6**).

To evaluate the optimal flow rate of the device, we used four different sample flow rates and collected the initial sample before processing, the effluent after exosome capture, and the sample after release. The quantity of exosomes captured and released have been calculated

based on the concentration differences between the initial sample and the sample following release. From the experiments with the PDMS block and small chambers, we did not see any difference in release concentration with change in flow rate. As a result, we fixed the release condition as 1ml/h, which is significantly higher than that for exosome capture. **Figure 3**c-d demonstrates that a capture flow rate of 900μL/hr offered the highest capture efficiency on average, but average release efficiency seemed to decrease for samples ran at this rate compared to two slower flow rates. At 1,200μL/hr, there was a decrease in capture efficiency with an additionally lowered release efficiency. This could imply that high flow rates lead to exosome capture that caused the device to become too congested for effective flow of EDTA and the subsequent vesicle release. However, 1200μL/hr did offer the highest specificity (**Figure 3**e), meaning a higher concentration of particles outside of the typical size range for exosomes collected at the outlet during sample processing. Both 300μL/hr and 600μL/hr offered a relatively even distribution of capture efficiency, release efficiency, and specificity. Because 600μL/hr offered higher capture and release efficiencies with minimal decrease in specificity (**Figure 3**f), it was deemed optimal for this study and applied to the [new]ExoChip.

2. 3. Comparison with tetraspanins based ExoChip devices

As the majority of immunoaffinity based exosome isolation methods use tetraspanin proteins as a target to capture, we compared our results with ExoChip devices conjugated with antibodies against the tetraspanin proteins CD63, CD9 and CD81 in terms of cancer-associated exosome capture and recovering performances (**Figure 4**).

First, using DiO staining we aimed to compare the exosome capture performance between the ^{new}ExoChip and the other immunoaffinity methods. Additionally, two devices, one with and one without avidin functionalization, were used as control devices after blocking. We used the same quantity of A549 exosome spiked in PBS as an initial sample and followed by DiO staining and additional washing. The staining showed considerably higher fluorescence intensities and bound particles on the device with annexin V mediated isolation compared to the other devices (**Figure 4**a). Again, the entire region of the device after DiO staining was scanned and we evaluated the relative fluorescence expression for each device (**Figure 4**b). The relative fluorescence intensity from the ^{new}ExoChip is considerably higher than other devices and the intensities from other tetraspanin based devices were similar to that of the avidin functionalized control ExoChip. In order to evaluate this result more quantitatively, we evaluated the capture performance of each device by comparison between initial exosome number and the resultant number after a capturing event. This quantitative comparison also yields significantly higher capture efficiencies on average for those devices functionalized with annexin V. The average capture efficiency for annexin V functionalized devices was found to be around 90% (**Figure 4**c), whereas the highest, average capture efficiency associated with an anti-tetraspanin device was found to be just over 40% for device conjugated with anti-CD63. Based on these results, the expression of phosphatidylserine on the surface of exosomal membranes is more reliable than the expression of these commonly used tetraspanins for A549 lung cancer cell derived exosome.

Next, we extended our study with three conditions, annexin V, anti-CD63 and a control device with avidin functionalization, and evaluated the quantity of exosomes captured and released using NTA (**Figure 4**d-e). After processing, exosomal concentration in the effluent

collected from the outlet of the ^{new}ExoChip was lowest in devices treated with annexin V, followed by those captured with anti-CD63, and greatest in the control devices that did not undergo any kind of surface modification. In other words, the control devices yielded the lowest capture efficiencies as expected given that the only means of capture is non-specific binding of particles within the devices.

Exosomal concentrations of collected samples follow the opposite trend, with annexin V devices yielding the highest mean concentration after EDTA release and anti-CD63 yielding a mean concentration marginally higher than that of the control devices. It follows that the annexin V recovery rate is notably higher than those of anti-CD63 and without antibodies. One would expect the concentration of exosomes in the device effluent after release for a device with antibody to be greater than the concentration after processing, as shown with annexin V; however, devices treated with anti-CD63 exhibit the opposite trend, speaking to the benefit of using reversible PS-annexin V reaction. Annexin V also offers the highest specificity towards vesicles in the exosome size-range within a relatively small range of values as compared to devices conjugated with anti-CD63 and those without any capturing molecules. These NTA results support previous DiO staining results.

2. 4. Device performance verification using model samples with healthy and cancer cell line-derived exosomes

After device optimization, we prepared several different exosome samples from different sources and evaluated the capturing ability of our device. These include exosomes from two lung cancer cell lines (A549 and H1975), two melanoma cell lines (SK103 and SK19) and a

normal lung fibroblast cell line (MRC5). Cell line derived exosomes were processed through the device after initial purification using ultracentrifugation and the exosomes were spiked into buffer solution at the concentration of 1×10^8 exosomes/ml for verification. All cancer cell-derived exosomes consistently yielded high capture efficiencies using the ^{new}ExoChip with an average capture efficiency of 90.19±5.70%. However, normal cell derived exosome showed a significantly lower capture efficiency of 38.43±15.80%. This could suggest that cancer cell derived exosome samples express more PS on their surfaces and therefore have a higher probability of binding to the annexin V compared to that of normal cell derived one. We also evaluated the recovery rate and specificity of the cell line exosomes, and they showed similar trends to the capture efficiency, with a lower recovery rate for MRC 5 exosomes than any others (**Figure 5**a). Even though MRC5 exosomal quantity after release was significantly lower than others, its purity was high. Interestingly, even though capture efficiency of H1975 was very high, its recovery rate was slightly lower than other cancer exosome cases, implying that release performance might vary depending on the source of the exosomes. After release, the size distribution of the released exosomes was carefully evaluated to see the differences between the sources of origin (**Figure 5**b). It is noteworthy that the average size of lung cancer cell derived exosomes was bigger than those of melanoma and normal cells. D-values of the lung cancer exosomes are also bigger than the others and it could be meaningful if further studies and verification are fulfilled.

2. 5. Isolation of exosomes from in-house lung cancer patient circulating tumor cell line supernatant and healthy donor exosome samples

Before the use of our devices with clinical samples, we prepared exosomes from two in-house lung cancer CTC lines to both determine the heterogeneity and the capture efficiencies of patient-derived exosomes. These two CTC cell lines originated from two different lung cancer patients, and their in-vitro supernatants without FBS were used as samples for our devices. The device without Av immobilization was used as a control device. After release, the release solution's exosomal concentration and size profiles were measured by NTA. In both cases, our devices isolated significantly higher quantities of exosomes than control devices (**Figure 6**a). However, the concentration and size profile were varied between exosomes derived from the two CTC lines. CTC-R1 derived exosomes shows higher concentration but smaller size profile compared to CTC-R2, showing the heterogeneity of exosomes depending on the sample (**Figure 6**b). As such, we can expect that the exosomal concentration and size will vary from patient to patient. In addition to this experiment, we also pre-purified an aliquot of CTC-derived exosomes samples using ultracentrifugation and used one purified healthy donor (HD) exosome sample (System Biosciences) to evaluate the recovery rates and purity after release using the [new]ExoChip. We then used the same concentration of each of the three different exosome samples to account for varying capture rates based on initial concentration. We could clearly see that the two CTC-derived exosomes show considerably higher recovery rate than the HD's exosomes, which is similar our cancer and normal cell line results (**Figure 6**c). Despite significant differences in exosomal concentration and sizes between the two CTC derived exosomes, their recovery rates are similar and remained high enough to be distinguished from HD exosomes.

2. 6. Performance comparison with conventional exosome isolation methods using model samples

Thus far, there are several exosome isolation methods commercially available and ultracentrifugation and polymer (PEG) based exosome kits have been widely used by many researchers due to the relatively low technical barrier. Therefore, we compared our ^{new}ExoChip's performance with these methods using multiple model samples. First, we used the model sample containing a known quantity of A549-derived exosomes spiked ($5x10^8$ exosomes/ml) in PBS buffer. Using the identical concentration and volume of the initial sample, our ^{new}ExoChip captured 67.26 % of spiked exosomes while ultracentrifugation captured only 5.52% of exosomes (**Figure 7**a). Ultracentrifugation has been widely accepted as a gold standard for exosome capture, however, it shows substantial sample loss during the multiple processing steps when the amount of target exosome is very limited.

Similarly, by using our in-house CTC cell line, CTCR1, derived media supernatant after removal of cellular debris, the ^{new}ExoChip yielded exosomal concentration and purity percentages of $4.26x10^8$ and 47.29% respectively as compared to ultracentrifugation which yielded $2.12x10^8$ and 89.6% (**Figure 7**b). Notably, the average purity of the sample after ultracentrifugation was higher than that for the ^{new}ExoChip, indicating lower selectivity compared to ultracentrifugation. However, as a whole, the recovered number of exosomes is still more effective with the ^{new}ExoChip, which will be more effective for determining accurate counts of exosomes within patient samples. At the same time, annexin V might capture apoptotic bodies expressing PS too, so it might be useful to remove bigger debris for clinical studies. The highest exosomal concentration was achieved using the PEG-based kit, at $1.28x10^9$ exosomes with a purity of 72.90%, both notably higher than those values for the

newExoChip. However, the NTA data suggests that this kit is not fully capable of capturing smaller vesicles (30-50nm) (**Figure S7**), which may make this method unreliable by way of excluding smaller sized exosomes for downstream analysis.

2. 7. Performance comparison with ultracentrifugation method using plasma samples

Using four different clinical plasma samples from cancer patients and healthy donors, we aimed to compare our exosome recovery performance with the gold standard ultracentrifugation method. We compared these results in terms of exosome-like vesicle recovery and sample purity after recovery (**Figure 7**c-d). In all cases, we used identical volumes of initial plasma samples and resuspended them in equal volume of buffer solution. From this study, other than one healthy donor (HC-D), the newExoChip captures significantly more exosomes than UC, and this tendency was more significant in two cancer cases (**Figure 7**c). Processing samples with the newExoChip offers higher purity than with ultracentrifugation for both healthy and cancer samples, as well as a significantly greater concentration of exosomal particles for cancer samples (**Figure 7**d). The present newExoChip appeared to be more effective when processing samples from cancer patients.

2. 8. Isolation of exosomes from plasma samples of cancer patients and healthy donors

We extended our study to 12 clinical plasma samples from lung (n=4), melanoma (n=3) and healthy donors (n=5). In all cases, we used 30-100µl of plasma samples for exosome isolation using our newExoChip. The concentration, size distribution, shapes, and proteins expression

levels of exosomes released from the device were evaluated using NTA, SEM, and western blot analysis. **Figure 8a** shows the various exosome concentrations for each patient and by cancer type. Although the 5 healthy donors show similar exosomal concentrations, the cancer patients showed a wide range of exosome concentrations. The *Ma* showed the highest (2.79×10^9/ml) and *Ld* showed the lowest concentration (2.89×10^8). Statistical analysis of particle size confirmed specificity of most samples, both cancerous and healthy (**Figure 8**b). While there is a wide range of particulate sizes captured, the mean size of every sample falls below 150nm in diameter, and the mode of each sample (excluding *Ld*) falls lower than the corresponding mean. Interestingly, the average size of exosomes from lung cancer was bigger than those of melanoma and healthy control. Similar size differences were shown in our cell line experiments. This could imply that lung cancer exosomes isolated by PS-annexin V affinity might be larger than usual or that another majority of extracellular vesicles in lung cancer might affect this size distribution. However, this information, along with the median values, showed that a considerable portion of samples collected from all sample types fall within the exosomal size range. The varying sizes of captured exosomes were also verified by SEM analysis (**Figure 8**c). In order to confirm that the captured vesicles from our device are exosomes, we used western blot analysis to verify the expression of exosomal markers. Instead of using CD63, which is known to have lower expression on lung cancer exosomes, we used CD9 and Flotillin-1 as exosomal markers. From the western blot analysis using three lung plasma samples and two melanoma samples, we see positive bands for both exosomal markers (**Figure 8**d). Additionally, the samples were probed for beta-actin as a standard loading control and calnexin to verify that there was no cellular contamination within the samples. [46, 47]

3. Conclusion

The present study showed that our PS targeting microfluidic device is capable of capturing tumor-associated exosomes more efficiently than the previous ultracentrifugation method and well-known exosomal protein marker method. Recently, one study of NSCLC exosomal lipids reported that several specific exosomal lipids might be useful markers for distinguishing advanced cancers from less advanced and normal. [48] Although most previous studies have focused on exosomal proteins, monitoring the exosomal lipids for alteration depending on the disease status might be more suited for clinical use. Even though we showed that our method facilitates effective exosome isolation, the exosomes isolated may be one subset of exosomes, which means this result and clinical meaning need to be interpreted with caution. This PS expression might not be specific to cancer only as some immune cell also might express PS during their progression. We captured natural killer cell line (NK-92MI) derived exosomes and we found that our device recovers more than 90% of spiked NK exosomes (Supplementary Information **S8**). In addition to PS expression of NK exosomes, the PS expression at the exosomal surface seems to also be related to the immune response of the body. Keller et al. showed that uptake of ovarian carcinoma exosomes by natural killer cells require PS on the exosomal surface, implying that PS expression is not only resulting feature during vesiculation but also may have certain roles to be regulated by other immune cells. [49] Exosomes from tumor cells have been shown to have the potential to induce antitumor activity, so their PS expression might help its activation. [50] Thus, the exosomes isolated using this PS-based method might be more effective to induce immune response, suggesting that this subset might be useful for further clinical use. Several prospective studies have showed that PS is expressed on cancer derived exosomes in ovarian cancer and prostate

cancer. In addition to these, our studies making use of PS expression on exosomes from lung cancer and melanoma is consistent with previous results. These results empower the theory that cancer exosomes express PS abundantly and may induce some immune response. The present ^{new}ExoChip facilitates the isolation of cancer-associated exosomes, thus allowing us to explore the undiscovered roles of exosomes in cancer progression and metastasis.

Experimental Section

Model sample preparation: In order to examine the performance of the ^{new}ExoChip, we prepared five different types of model samples depending on the aim of the study. For the evaluation of device performance in lung cancer, we prepared two different cell line derived exosomes, A549 and H1975 derived exosomes. For A549-derived exosomes, we purchased A549-derived exosomes (SBI) in the concentration of $1x10^{10}$/ml (NTA) and diluted them into 1x binding buffer solution. For H1975-derived exosome, we cultured the H1975 under the standard cancer cell culture conditions using exosome-depleted fetal bovine serum (FBS), and ultracentrifuged the supernatant to isolate the exosomes. After ultracentrifugation, we measured the concentration using NTA, and a known number of exosomes was used for model sample preparation. In every case for ^{new}ExoChip, we used annexin V binding buffer 1x as a basic buffer. For the comparison study with anti-CD63, we used the same exosome concentration but diluted them into standard PBS solution. Two patients' CTC derived cell lines were additionally prepared to examine our device's potential for clinical use. Similar to preparation of cancer cell line-derived exosomes, those CTC-derived cell lines were cultured with in-house media with exosome-depleted FBS for 1-3 days, and their supernatants were processed by our devices.

Human plasma sample preparation: The sample collection and experiments were approved by University of Michigan Institutional Review Board (IRB). Informed consents were obtained from all participants of this clinical study and NSCLC and melanoma blood samples were obtained after approval of the institutional review board at the University of Michigan. All experiments were performed in accordance with the approved guidelines and regulations by the ethics committee at the University of Michigan. Each blood sample was centrifuged at 2,000g for 15 minutes to sediment all cells, and then at 12,000g to remove all residual cellular debris. After centrifugation, the supernatant was gently collected and stored at -80°C.

PS-Annexin V binding affinity evaluation: For the initial verification of binding affinity between cancer cell-derived exosomes and annexin V, we immobilized the biotinylated-annexin V onto small chamber devices and square PDMS blocks (Annexin V block) by standard avidin-biotin conjugation methods. For the negative control, identical device and block without annexin V functionalization (blank block) were used. The anti-CD63 conjugated PDMS device/block (CD63 block) was used as positive control. For the chamber device, static or dynamic sample processing was placed. For dynamic sample processing, 200µl of model sample containing DiO stained A549-derived exosomes was gently flowed through the device using a syringe pump at the flow rate of 0.3ml/hr and non-bound exosomes were washed out with the flow rate of 0.5ml/hr. For the release, 20mM EDTA was flowed through at the flow rate of 0.9ml/hr. For the static sample processing, 50µl of non-diluted DiO-A549 stock solution was statically pipetted and incubated for more than 12 hours in 4°C. The chamber was washed out by pipetting additional binding buffer solution and 20mM EDTA solution was used for the release process. Similar to the static chamber

experiments, PDMS blocks with/without capturing molecules were exposed to DiO stained A549 exosome stock solution and incubated 1 hour for the capturing process. For the release, 10-20mM EDTA solution was used. For every step, the devices before/after capture and after release were examined under a fluorescence microscope and evaluated by its relative fluorescence.

Device design, numerical analysis and fabrication: The [new]ExoChip device has 30 ripple-shaped channels, and each channel is composed of 60 circular channels in a row. Each circle has a diameter of 500μm and the distance between each circle is 900μm. The junction between two adjacent circular patterns has a width of 75μm. The channels repeatedly expanding and shrinking are ideally designed for enhancing binding affinity between samples and antibody-conjugated patterns. The height of the patterns was designed to be 50μm. We have confirmed that these channels increase the binding chance between exosomes and annexin V conjugated channels by decreasing flow velocity and increasing surface area. These results were found using numerical analysis performed in COMSOL (Supplementary Information **S1)**. The [new]ExoChip is fabricated by standard soft-lithography including mold fabrication and PDMS molding (Supplementary Information **S2)**. By patterning SU8-2050 photoresist on a silicon wafer, we prepared the [new]ExoChip mold and its height of 58.67±2.25μm was confirmed by alpha-step measurement. By pouring PDMS and PDMS curing agent mix (1:10), PDMS mold was fabricated and the prepared PDMS pattern was bonded to clean slide glass by O_2 plasma treatment.

Surface modification: For the surface modification on the device, we used standard avidin-biotin chemistry with optimization.[11, 17] To elaborate, after plasma bonding between PDMS layer and slide glass, we injected silane solution (3ml Ethanol + 120µl Silane) three times and incubated 20 minutes after each injection. The devices were then injected and flushed out with ethanol as a washing step. Next, the devices were injected with a GMBS mixture (2ml Ethanol + 6µl GMBS) two times and incubated 15 minutes after each injection. Again, the devices were flushed out with ethanol. Following the second washing step, the devices were injected with Avidin (1ml of filtered PBS + 100µl of NeutrAvidin), placed in a Petri dish sealed with parafilm along with wet paper napkins, and incubated overnight in a standard refrigerator. After 1-10 days, the devices were defrosted and washed out with filtered PBS. Before the biotinylated annexin V conjugation, we checked and confirmed the coverage of avidin in our device using biotinylated staining dye (Supplementary Information **S3**). The devices were then injected with 110µl of the biotinylated annexin V (10µl annexin V + 100µl of 1x Binding Buffer): 55µl into the inlet, a 30-minute incubation period, 55µl into the outlet, and another 30-minute incubation period before use. Biotinylated annexin V has been incorporated with various avidin-conjugated substrates. [51-53]

Devices used for comparison studies with anti-CD63, anti-CD81, and anti-CD9 have been prepared by standard biotin-avidin antibody conjugation methods. The devices were injected with 100 µl of the biotinylated antibodies (2 µl biotin antibody solution+98 µl of PBS) the same way as with annexin V and washed with PBS. Devices used for controls were prepared in two ways: 1) followed by avidin functionalization and 2) without any functionalization. All control devices were injected with 3% BSA solution (0.03g/1ml filtered PBS) to prevent nonspecific binding and were incubated for at least 30 minutes before use.

Sample processing-exosome capture and release: The prepared model samples or patient plasma samples were processed using a Harvard syringe pump at the flow rate of 0.3-1.2ml/hr. All samples were prepared in the 1x of binding buffer containing 2.5mM of $CaCl_2$ to be actively conjugated with annexin V. 300ul of sample was withdrawn into a 1ml syringe and connected to the device. After exosome capture, 200μl of 1x binding buffer was processed at the flow rate of 1ml/hr to remove the excess unbound vesicles/proteins. For the release of the captured exosomes, 300μl of 20mM EDTA solution was flowed at the flow rate of 1ml/hr in two steps; the 1st 150μl injection and 30minutes incubation without flow. Another 150μl was flowed and 200μl of PBS buffer injection was followed at the flow rate of 1ml/hr to make sample 500μl in total. The samples of 500μl after capture and release were analyzed quantitatively by nanoparticle tracking analysis (NTA).

Field emission scanning electron microscopy (FE-SEM): Immediately following capture and release experiments, small portions of each device were extracted using a biopsy punch and each punched PDMS specimen was fixed in 2.5% glutaraldehyde in PBS for one hour and then rinsed for 20 min with PBS, followed by dehydration with standard ethanol gradients solution (50%, 70%, 90%, 95%, and 100%). The specimen was then immersed for 10 min in a solution of ethanol/HMDS (1:1) and then transferred to 100% HMDS, followed by overnight air drying in the hood. The dehydrated specimen was then attached to carbon double sided tape, mounted on a SEM stub, and coated with gold by sputtering. Devices after capture and release were examined by FEI Nova 200 Nanolab Dualbeam FIB scanning electron microscope under low beam energies (2.0-5.0 kV) at the Electron Microscopy Analysis Lab (MC2) at University of Michigan.

DiO staining of the extracellular vesicles: Staining of extracellular vesicles using lipophilic dyes such as DiO and PKH has been used in various studies. [11,14,15] DiO staining was conducted in two experiments. First, the DiO stained A549 derived exosomes were prepared for the model sample experiment. In order to make DiO stained exosomes, 1μl of DiO staining dye (ThermoFisher, USA) was thoroughly mixed with 300μl of stock solution of A549 exosomes. After 20 minutes of incubation, ultracentrifugation was performed to remove excess dye. After another ultracentrifugation for exosome purification, the precipitated pellet was suspended with PBS and stored in a deep freezer until use (Supplementary Information **S4**). For the second experiment, direct DiO staining was conducted for quantitative analysis of the exosome capture/release. DiO staining was carried out after the normal sample processing and washing procedure with no release. 1μl of dye was added to 200μl of buffer (binding buffer for ^newExoChip, PBS for controls). Each device was injected with 200μl of the dye solution at a flow rate of 1,000μl/hr and incubated for 20 minutes without flow. This was followed with a second wash at 1,000μ/h with buffer solution to remove excess dyes. The binding tendency and amount were evaluated under fluorescence microscopy LV100 (Nikon, Japan). To compare the quantity of DiO stained exosomes captured on each device, the average fluorescent intensity was calculated using Nikon's NIS Elements software. The average background from each device was then subtracted to calculate a standardized average fluorescent intensity. The standard deviation was calculated using the variation in average intensities across each device.

Ultracentrifugation: Ultracentrifugation was used for two reasons: comparison study with [new]ExoChip and DiO-stained EV preparation. EVs were isolated using two different ultracentrifuge, Sorvall ultracentrifuges (ThermoFisher, USA) and Airfuge ultracentrifuge (Beckman Coulter, USA), depending on the sample volume. For the comparison study of model samples, the initial volume was 200μl and we used the Airfuge ultracentrifugation using an A-100/40 angle rotor for 30 minutes at 100,000xg. After the first centrifugation, 170μl of supernatant was removed from the tube and replaced with 170μl of pre-filtered PBS, and then followed by another same centrifugation step. For the comparison study of clinical samples, the same volume of initial plasma sample was used but diluted into PBS buffer. After initial ultracentrifugation at 100,000xg for 90 minutes, we aspirated the supernatant and injected another 38ml of PBS for 2nd centrifugation at 100,000 g for 90 minutes. The pellet after the 2nd centrifugation was gently spiked into 100μl of PBS and compared to the resultant from [new]ExoChip. For the preparation of DiO stained EV, we used the same rpm conditions but performed an additional centrifugation to remove excess dye debris.

PEG-based exosome isolation kit: For the comparison study, a polymer-based exosome isolation kit, Total Exosome Isolation Reagent (ThermoFisher, USA), was used. The isolation of exosomes with the kit was prepared by following the user manual of the kit. Briefly, the CTC cell line culture media was centrifuged at 2000xg for 30 minutes to remove cells and debris and 200μl of the media supernatant was gently mixed with 100μl of the reagent. The mixed sample was incubated at 2°C overnight and after incubation, we centrifuged the sample at 10,000xg for 1 hour at 4°C. Then, the exosome pellet was resuspended with PBS for NTA analysis. Each experiment was carried out in triplicate.

Nanoparticle tracking analysis: For the evaluation of the concentration and the size distribution of the resultant effluent, nanoparticle tracking analysis (NTA) was performed using the NanoSight NS300 (Marven Instruments, UK). 30μl of the resultant was used and a laser module was mounted inside the main instrument housing. Based on the Brownian motion of nanoparticles, this equipment visualizes the scattered lights from the particles of interest. This movement was monitored through a video sequence for 20 seconds in triplicate. All data acquisition and processing were performed using NanoSight NS300 control software. (Screen gain: 7, camera level: 13, detection threshold: 5)

On-chip protein extraction and western blot analysis: Exosome lysis was performed using RIPA buffer with 1% protease inhibitor. The prepared buffer solution was flowed through the device at the flow rate of 50μL/min right after exosome isolation. Initially we injected 40μL of sample to remove residual solution in the device and started sample collection after 40μl. This was immediately followed by an injection of 50μL per device at the same rate. Devices were incubated for 5 minutes, and then injected with another 50μL at 50μL/min. Finally, devices were manually injected with air to push out as much sample as possible from each device. The collected samples were then gently dispersed by vortex mixer and kept in -20 °C.

Total protein was measured by standard BCA analysis according to the manufacturer's instructions. For the released sample, we used microBCA analysis because its high concentration in EDTA is not compatible to standard BCA analysis. Western Blot analysis was performed on a precast 4-20% SDS gel from BioRad. The samples were prepared in 4x Laemelli buffer with 2-mercaptoethanol and heated to 95°C for 5 minutes before loading onto the gel. The gel was run at 120V for 1 hour before transferring at 120V for 1 hour 15

minutes on ice. Blocking was performed in 5% non-fat milk in TBST for 90 minutes.

Primary antibodies were incubated overnight on a rocker at 4°C at a concentration of 1:500

(Flotillin-1, Santa Cruz), 1:1000 (CD9, Cell Signaling; Calnexin, Cell Signaling), or 1:1500

(Beta-Actin, Cell Signaling) in 3% non-fat milk in TBST. Thorough rinsing was performed,

and then secondary antibody was incubated for 2 hours at room temperature (anti-Mouse,

Santa Cruz; anti-Rabbit HRP, Cell Signaling) at 1:1500 in 3% non-fat milk in TBST.

Supporting Information
Supporting Information is available from the Wiley Online Library or from the author.

Acknowledgements

<div align="right">
Received: ((will be filled in by the editorial staff))
Revised: ((will be filled in by the editorial staff))
Published online: ((will be filled in by the editorial staff))
</div>

Reference

[1] M. Simons, G. Raposo, *Curr. Opin. Cell. Biol.* 2009, 21, 575.

[2] P.B. Devhare, R. Sasaki, S. Shrivastava, A.M. Di Bisceglie, R. Ray, P.B. Ray, *J. Virol* 2017, 91(6), e02225.

[3] B.N. Hannafon, W.Q. Ding, *IJMS* 2013, 14(7), 14240.

[4] T.L. Whiteside, *Adv Clin Chem* 2016, 74, 103.

[5] H. Zhao, L. Yang, J. Baddour, A. Achreja, V. Bernard, T. Moss, J.C. Marini, T. Tudawe, E.G. Seviour, F.A. San Lucas, H. Alvarez, S. Gupta, S.N. Maiti, L. Cooper, D. Peehl, P.T. Ram, A. Maitra, D. Nagrath, *Elife* 2016, e10250.

[6] A. Hoshino, B. Costa-Silva, T.L. Shen, G. Rodrigues, A. Hashimoto, M.T. Mark, H. Molina, S. Koshaka, A. Di Giannatale, S. Ceder, S. Singh, C. Williams, N. Soplop, K. Uryu, L. Pharmer, T. King, L. Bojmar, A.E. Davies, Y. Ararso, T. Zhang, H. Zhang, J. Hernandez, J.M. Weiss, V.D. Dumont-Cole, K. Kramer, L.H. Wexler, A. Narendran, G.K. Schwartz, J.H. Healey, P. Sandstrom, K.J. Labori, E.H. Kure, P.M. Grandgenett, M.A. Hollingsworth, M. de Sousa, S. Kaur, M. Jain, K. Mallya, S.K. Batra, W.R. Jarnagin, M.S. Brady, O. Fodstad, V. Muller, K. Pantel, A.J. Minn, M.J. Bissell, B.A. Garcia, Y. Kang, V.K. Rajasekhar, C.m. Ghajar, I. Matei, H. Peinado, J. Bromberg, D. Lyden, *Nature* 2015, 527, 329.

[7] P. Li, M. Kaslan, S.H. Lee, J. Yao, Z. Gao, *Theranostics* 2017, 7(3), 789

[8] M.Y. Konoshenko, E.A. Lekchnov, A.V. Vlassov, P.P. Laktionov, *Biomed Res. Int.* 2018, 8545347, 27

[9] M. Szajnik, M. Derbis, M. Lach, P. Patalas, M. Michalak, H. Drzewiecka, D. Szpurek, A. Nowakowski, M. Spaczynski, W. Baranowski, T.L. Whiteside, *Obstet Gynecol* 2013, S4

[10] M. An, I. Lohse, Z. Tan, J. Zhu, J. Whu, H. Kurapati, M.A. Morgan, T.S. Lawrence, K.C. Cuneo, D.M. Lubman, *J Proteome Res* 2017, 16(4), 1763

[11] S.S. Kanwar, C.J. Dunlay, D.M. Simeone, S. Nagrath, *Lab Chip* 2014, 14(11), 1891

[12] Y.T. Kang, Y.J. Kim, J. Bu, Y.H. Cho, S.W. Han, B.I. Moon, *Nanoscale* 2017, 9(36), 13495

[13] Nano DLD, B.H. Wunsch, J.T. Smith, S.M. Gifford, C. Wang, M. Brink, R.L. Bruce, R.H. Austin, G. Stolovitsky, Y. Astier, *Nat. Nanotechnol.* 2016, 11, 936.

[14] P. Zhang, X. Zhou, M. He, Y. Shang, A. L. Tetlow, A. K. Godwin, Y. Zeng, Nat. Biomed. Eng. 2019, 3, 438-451

[15] J. Wang, W. Li, L. Zhang, L. Ban, P. Chen, W. Du, X. Feng, B.-F. Liu, ACS Appl. Mater. Inter. 2017, 9, 27441-27452

[16] X. Lv, Z. Geng, Y. Su, Z. Fan, S. Wang, W. Fang, H. Chen, Langmuir 2019, 35, 9816-9824

[17] Y.-T. Kang, E. Purcell, T. Hadlock, T.-W. Lo, A. Mutukuri, S. Jolly, S. Nagrath, Analyst 2019, DOI: 10.1039/C9AN01235D

[18] H. Lee, H. Im, H. Shao, Y.I. Park, V.M. Peterson, C.M. Castro, R. Weissleder, H. Lee, *Nat. Nanotechnol.* 2014, 32, 490.

[19] R. Qi, G. Zhu, Y. Wang, S. Wu, S. Li, D. Zhang, Y. Bu, G. Bhave, R. Han, X. Liu, *Biomed. Microdevices* 2019, 21, 35.

[20] S. Fang, H. Tian, X. Li, D. Jin, X. Li, J. Kong, C. Yang, X. Yang, Y. Lu, Y. Luo, B. Lin, W. Niu, T. Liu, *Plos One* 2017. 12(4), e0175050.

[21] C. Chen, J. Skog, C.H. Hsu, R.T. Lessard, L. Balaj, T. Wurdinger, B.S. Carter, X.O. Breakefield, M. Toner, D. Irimia, *Lab Chip* 2010, 10, 505.

[22] K. Lee, K. Fraser, B. Ghaddar, K. Yang, E. Kim, L. Balaj, E.A. Chiocca, X.O. Breakefield, H. Lee, R. Weissleder, *ACS Nano* 2018, 12(1), 494.

[23] B. Sandfeld-Paulsen, N. Aggerholm-Pendersen, R. Bæk, K.R. Jakobsen, P. Meldgaard, B.H. Folkersen, T.R. Rasmusen, K. Varming, M.M. Jørgensen, B.S. Sorensen, *Mol. Oncol.* 2016, 10(10), 1595

[24] M. He, J. Crow, M. Roth, Y. Zeng, A.K. Godwin, *Lab Chip* 2014, 14, 3773

[25] E. Reátegui, K.E. van der Vos, C.P. Lai, M. Zeinali, N.A. Atai, B. Aldikacti, F.P. Floyd Jr., A.H. Khankhel, V. thapar, F.H. Hochberg, L.V. Sequist, B.V. Nahed, B.S. Carter, M. Toner, L. Balaj, D.T. Ting, X. O. Breakefield, S. L. Stott, *Nat. Comm.* 2018, 175

[26] T. An, S. Qin, Y. Xu, Y. Tang, Y. Huang, B. Situ, J.M. Inal, L. Zheng, *J. Extracell. Vesicles* 2015, 4, 27522.

[27] R. Vaidyanathan, M. Naghibosadat, S. Rauf, D. Korbie, L.G. Carrascosa, M.J.A. Shiddiky, M. Trau, *Anal. Chem.* 2014, 86 (22), 11125.

[28] T. Skotland, K. Sandvig, A. Llorente, *Prog. Lipid Res.* 2017, 66, 30.

[29] M. Miyanishi, K. Tada, M. Koike, Y. Uchiyama, T. Kitamura, S. Nagata, *Nature* 2007, 450 (7168), 435.

[30] C. Thery, M. Ostrowski, E. Segura, *Nat. Rev. Immunol* 2009, 9(8), 581.

[31] R. Kim, M. Emi, K. Tanabe, *Cancer Biol. Ther.* 2005, 4(9), 924.

[32] D.D. Taylor, C. Gercel-Taylor, Semin. *Immunopathol.* 2011, 33(5), 441.

[33] T.J. Desai, J.E. Toombs, J.D. Minna, R.A. Brekken, D.G. Udugamasooriya, *Oncotarget* 2016, 7(21), 30678.

[34] J. Lea, R. Sharma, F. Yang, H. Zhu, E.S. Ward, A.J. Schroit, *Oncotarget* 2017, 8(9), 14395.

[35] W. Nakai, T. Yoshida, D. Diez, Y. Miyatake, T. Nishibu, N. Imawaka, et al., *Sci. Rep.* 2016, 6, 33935.

[36] X. Wei, C. Liu, H. Wang, L. Wang, F. Xiao, Z. Guo, et al., *PLoS One* 2016, 11, e0147360.

[37] P. Meers, T. Mealy, *Biochemistry* 1993, 32(43), 11711.

[38] H. Xu, C. Liao, P. Zuo, Z. Liu, B.C. Ye, *Anal. Chem.* 2018, 90(22), 13451.

[39] G. Rabinowits, C. Gerçel-Taylor, J.M. Day, D.D. Taylor, G.H. Kloecker, *Clin. Lung Cancer* 2009, 10(1), 42.

[40] P. Sharma, S. Ludwig, L. Muller, C.S. Hong, J.M. Kirkwood, S. Ferrone, T.L. Whiteside, *J. Extracell. Vesicles* 2018, 7, 1435138.

[41] K. Denzer, M. J. Kleijmeer, H. F. G. Heijnen, W. Stoorvogel and H. J. Geuze, *J. Cell Sci.* 2000, 113, 3365-3374.

[42] C. Thery, L. Zitvogel, S. Amigorena, *Nat Rev Immunol,* 2002, 2, 569.

[43] W. Oosthuyzen, N. E. Sime, J. R. Ivy, E. J. Turtle, J. M. Street, J. Pound, L. E. Bath,

D. J. Webb, C. D. Gregory, M. A. Bailey and J. W. Dear, *J. Physiol.* 2013, 591, 5833.

[44] V. Prachayasittikul, C. Isarankura-Na-Ayudhya, T. Tantimongcolwat, C. Nantasenamat, H.-J. Galla, *ABBS* 2007, 39, 901.

[45] D. M. Wong, T. T. N. Nguyen, A. K. Franz, *Algal Res.* 2014, 5, 158.

[46] T. S. Martins, J. Catita, I. M. Rosa, O. A. B. da Cruz e Silva, A. G. Henriques, PLoS One 2018, 13(6), e0198820

[47] C. Lässer, M. Eldh, J. Lötvall, J. Vis. Exp. 2012, 59, 3037.

[48] T.W.M. Fan, X. Zhang, C. Wang, Y. Yang, W.Y. Kang, S. Arnold, R.M. Higashi, J. Liu, A.N. Lane, *ABBS* 2018, 1037, 256.

[49] S. Keller, A.K. Konig, F. Marme, S. Runz, S. Wolterink, D. Koensgen, A. Mustea, J. Sehouli, P. altevogt, *Cancer Lett.* 2009, 278, 73.

[50] J. Wolfers, A. Lozier, G. Raposo, A. Regnaulat, C. Thery, C. Masurier, C. Flament, S. Pouzieux, F. Faure, T. Tursz, E. Angevin, S. Amigorena, L. Zitovogel, *Nat. Med.* 2001, 7, 297.

[51] Y. Pan, W. Shan, H. Fang, M. Guo, Z. Nie, Y. Huang, S. Yao, *Biosens Bioelectron* 2014, 52, 62-68.

[52] H. Montón, M. Medina-Sánchez, J. A. Soler, A. Chałupniak, C. Nogués, A. Merkoçi, Biosens. Bioelectron. 2017, 94, 408-414.

[53] J. H. Rand, X. –X. Wu, H. A. M. Andree, J. B. A. Ross, E. Rusinova, M. G. Gascon-Lema, C Calandri, P. C. Harpel, Blood 1998, 92, 1652-1660.
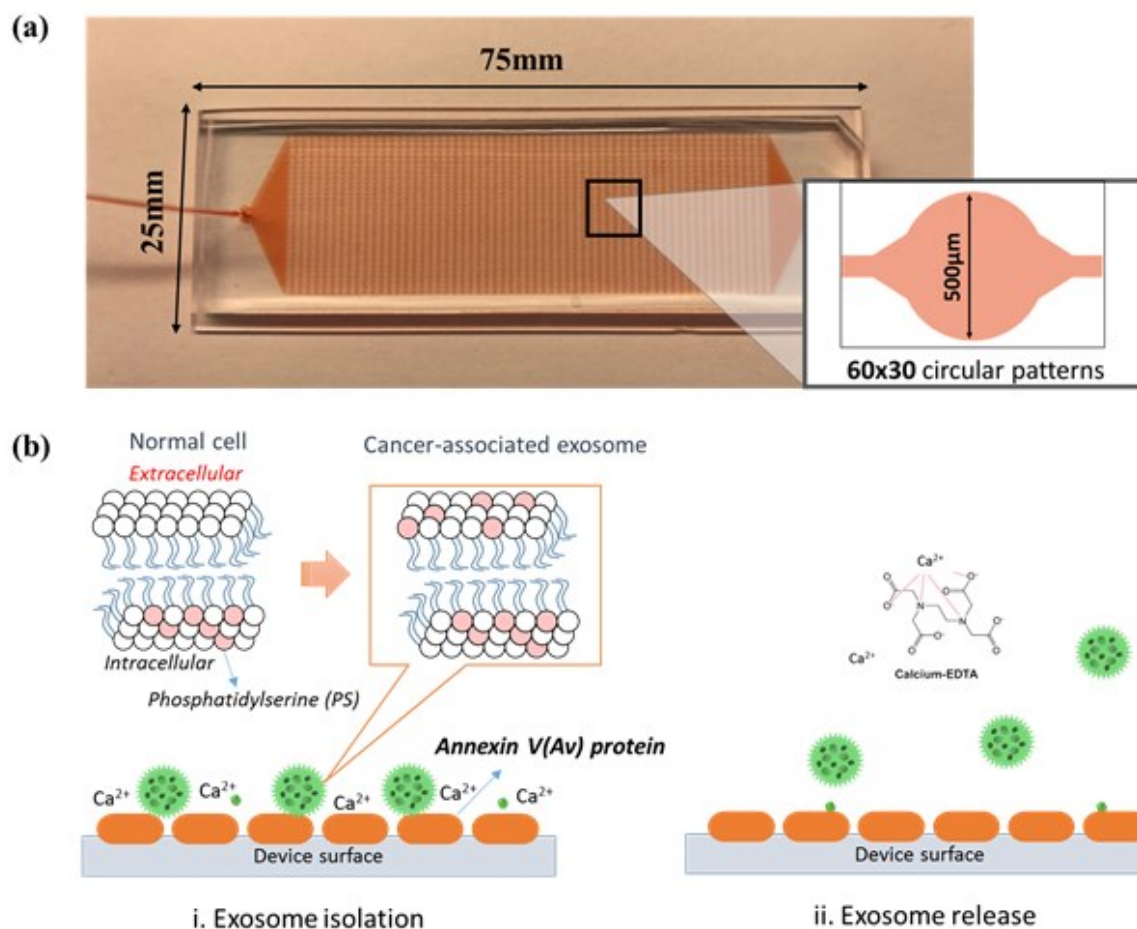
Figure 1. ^{new}ExoChip design and working principle. **a)** The fabricated ^{new}ExoChip features 30 by 60 circular patterns with a diameter of 500μm in standard slide glass size. **b)** the mechanism of the capture and release of cancer-associated exosomes using Ca^{2+} dependent binding between PS and annexin V and EDTA-based Ca^{2+} chelation, respectively.

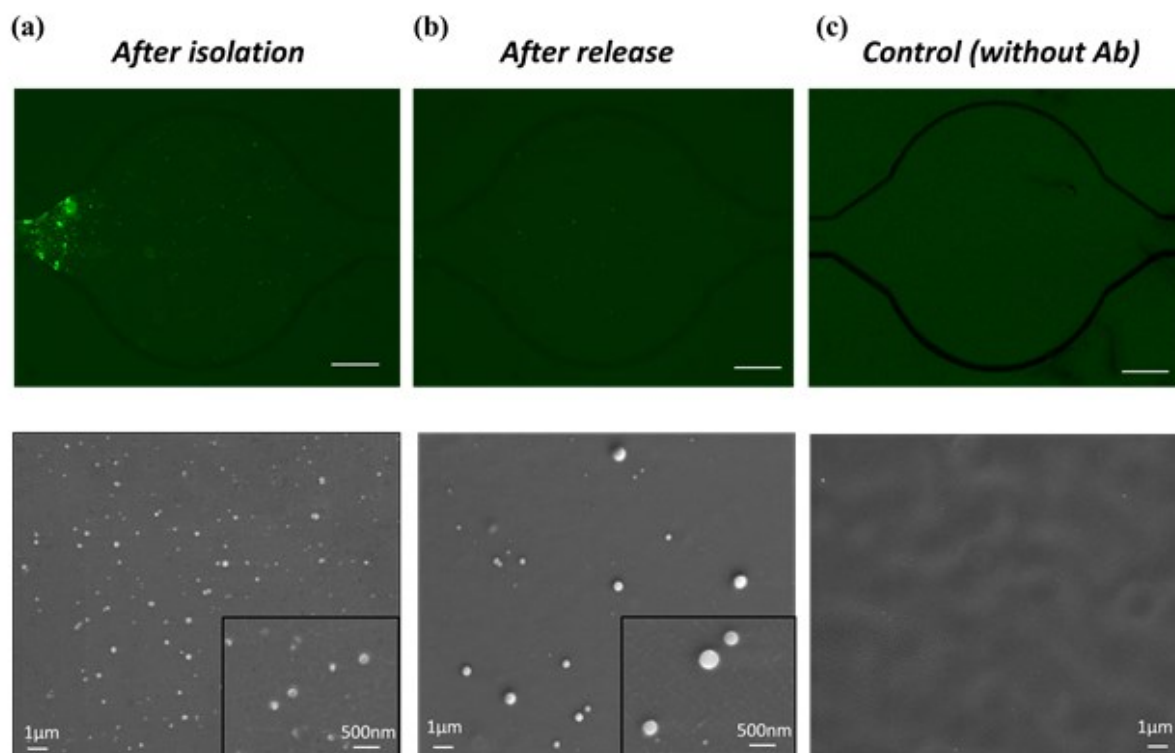**Figure 2.** DiO staining and SEM microscopy analysis for confirmation of exosome capture and release using DiO stained A549-derived cancer exosome sample. **a)** a fluorescent image of a circular pattern (*Scale bar=100μm*) (top) and a SEM image of the surface on pattern (bottom) after isolation, **b)** after release, and **c)** control device after capture. All devices use same amount of A549 exosomes.
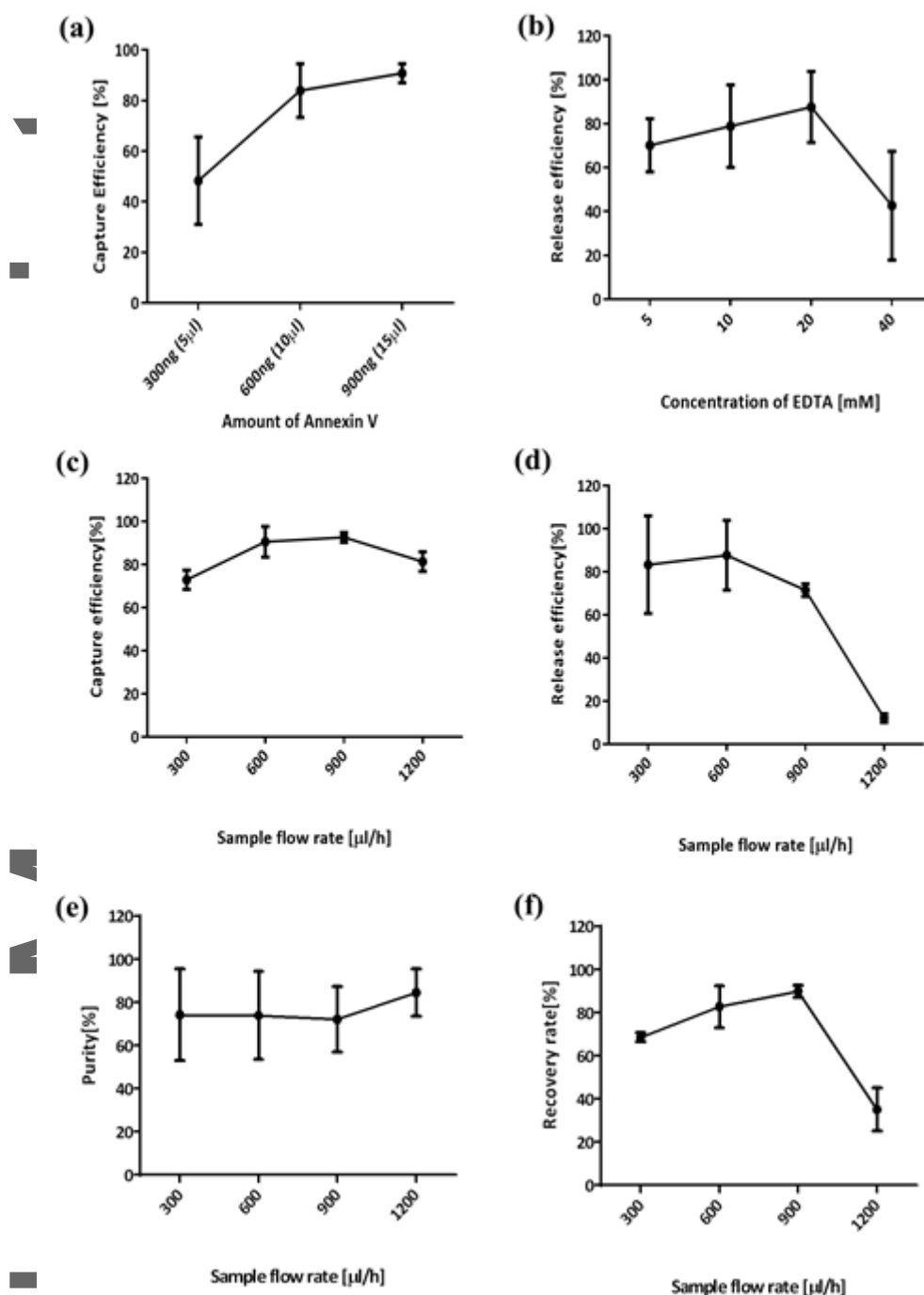
Figure 3. Device optimization using A549-derived exosome samples. **a)** amount of biotinylated annexin V for functionalization. **b)** concentration of EDTA solution to release. **c-f)** finding optimal flow rate for sample processing in terms of **c)** capture efficiency, **d)** release efficiency, **e)** specificity of released sample and **f)** recovery rate.
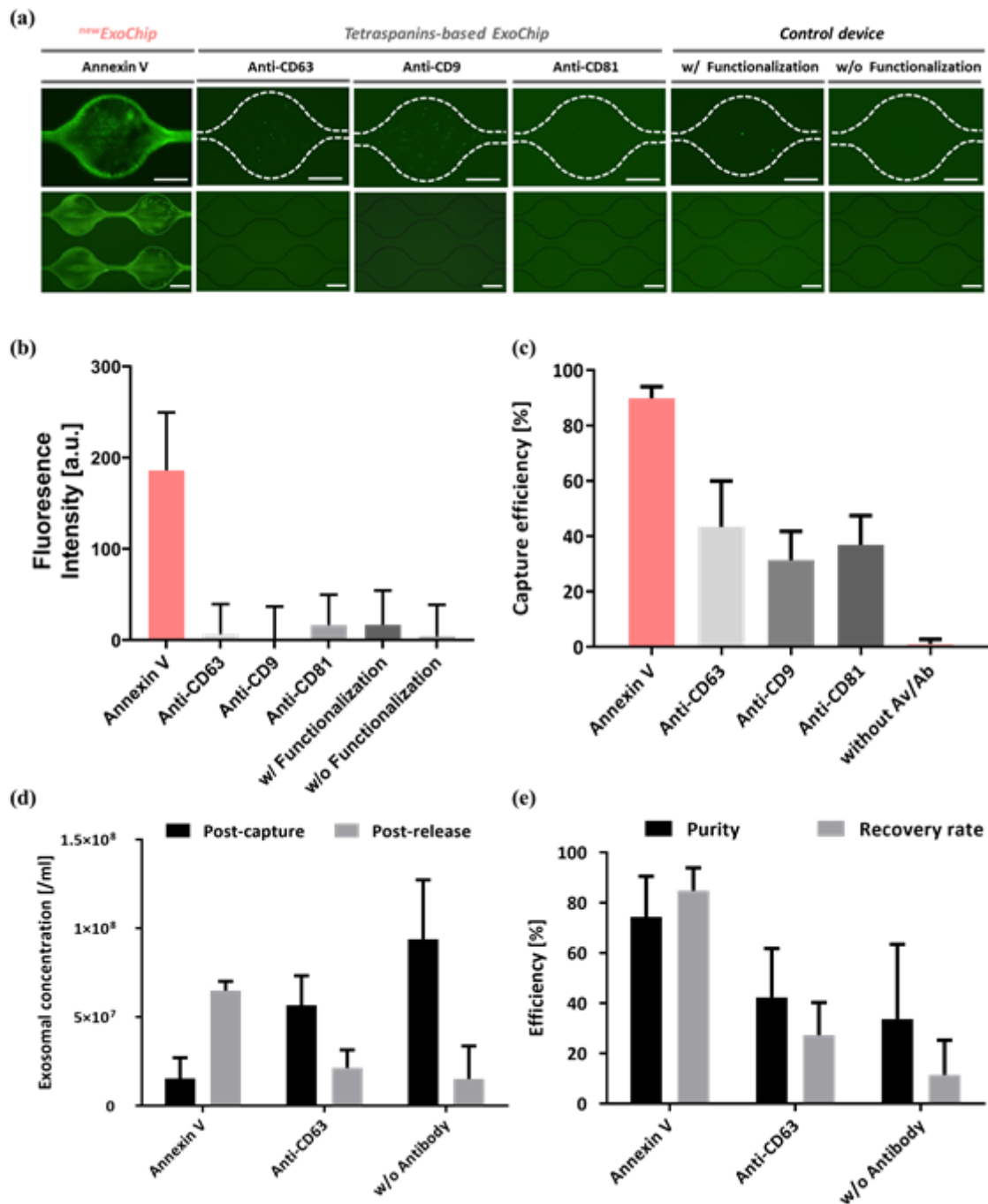
Figure 4. The comparison of the exosome recovery between Annexin-V based newExoChip and anti-tetraspanins based ExoChip. **a)** A549 exosome isolation performance comparison based on DiO staining (*Scale bar=200μm*). **b)** fluorescence intensity of each device after DiO staining. **c)** A549 capture efficiencies based on nanoparticle tracking analysis (NTA). **d-e)** A549 exosome isolation performance comparison based on nanoparticle tracking analysis.
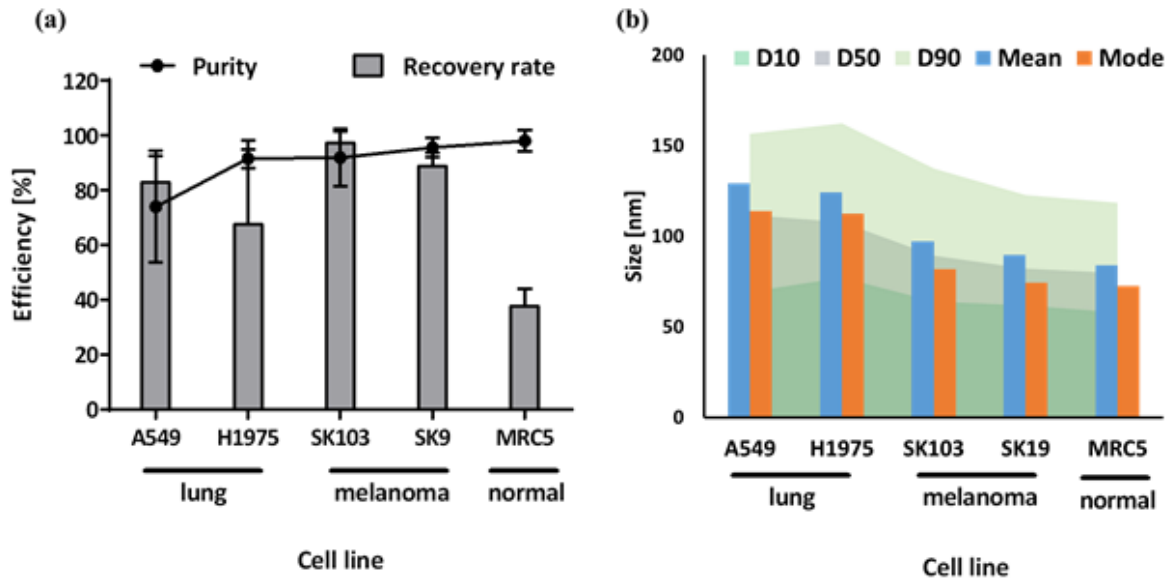
Figure 5. Cancer cell and normal cell derived exosome recovery using ᶰᵉʷExoChip. **a)** recovery rates and specificities of five different cancer/normal cell derived exosome samples. **b)** size distribution analysis in terms of mean, mode, and *D*-values (*D*10, *D*50, and *D*90) after release of exosomes using ᶰᵉʷExoChip.
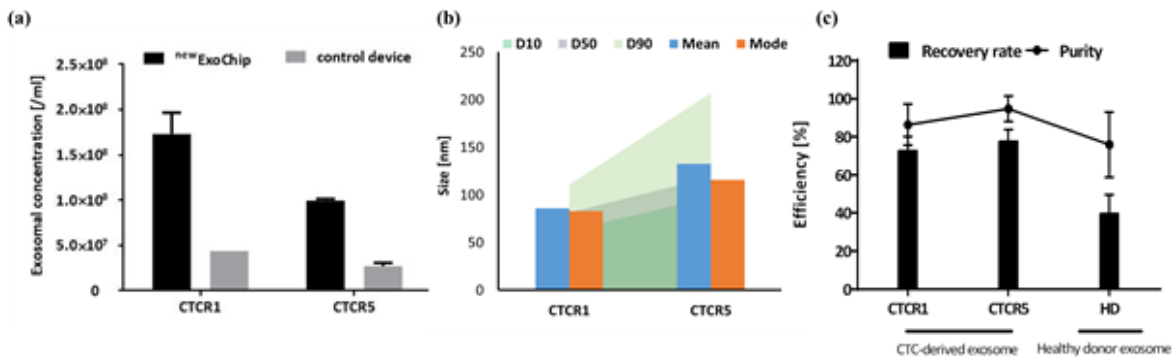

Figure 6. The in-house lung cancer circulating tumor cells (CTC) line-derived exosome isolation using ᶰᵉʷExoChip. **a)** exosome concentration after release using present devices and control devices. **b)** size distribution analysis of vesicles recovered by ᶰᵉʷExoChip. **c)** recovery rates and specificities of CTC-derived exosomes and comparison to healthy donor plasma exosomes using ᶰᵉʷExoChip.
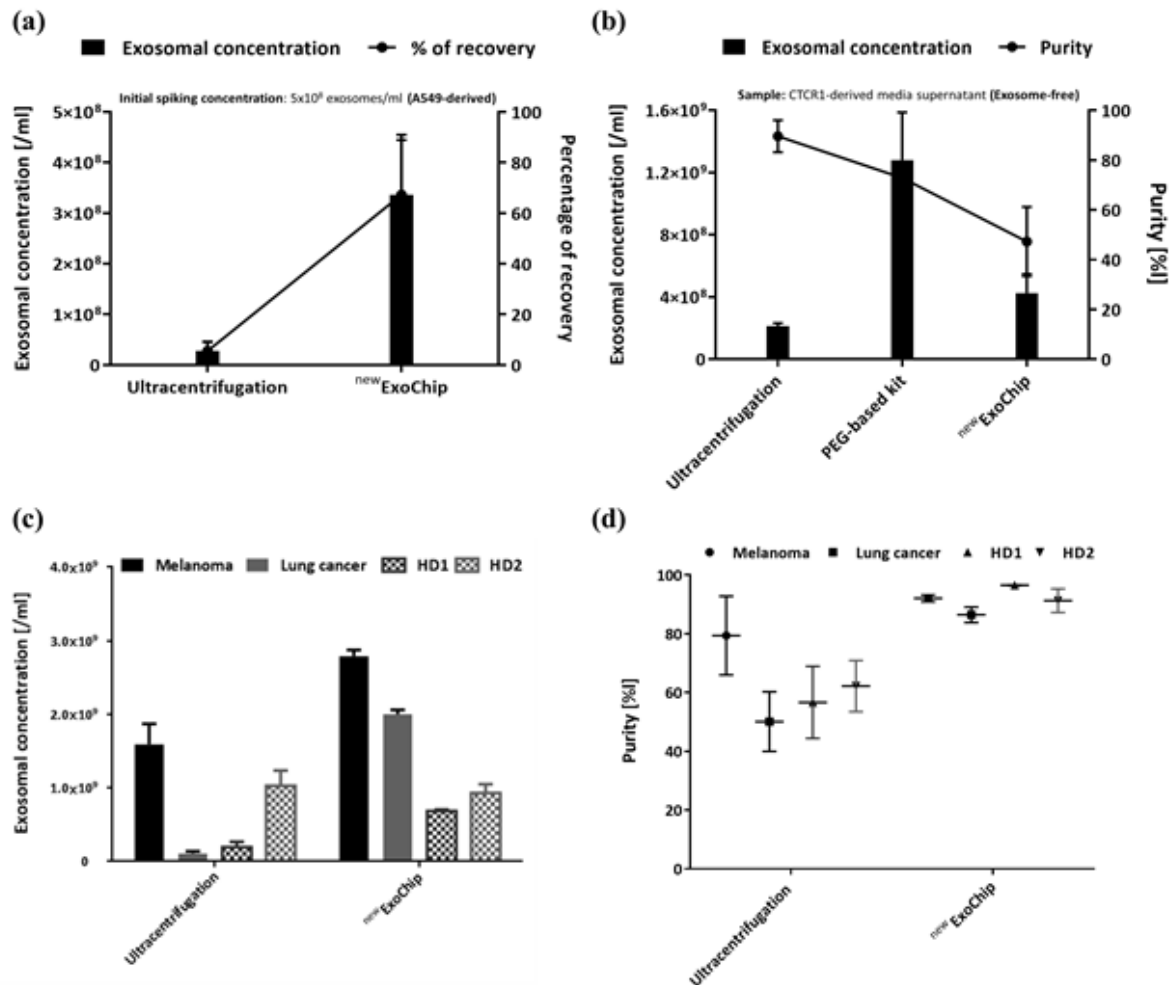
Figure 7. The exosome isolation performance between ^{new}ExoChip and conventional exosome isolation methods. **a)** comparison by using A549 exosomes spiked in PBS. **b)** comparison by using CTC cell line culture supernatant. **c-d)** comparison of the exosome recovery between ^{new}ExoChip and ultracentrifugation using clinical samples. exosomal concentration after recovery **(c)** and purity of the recovered samples after isolation **(d)**.
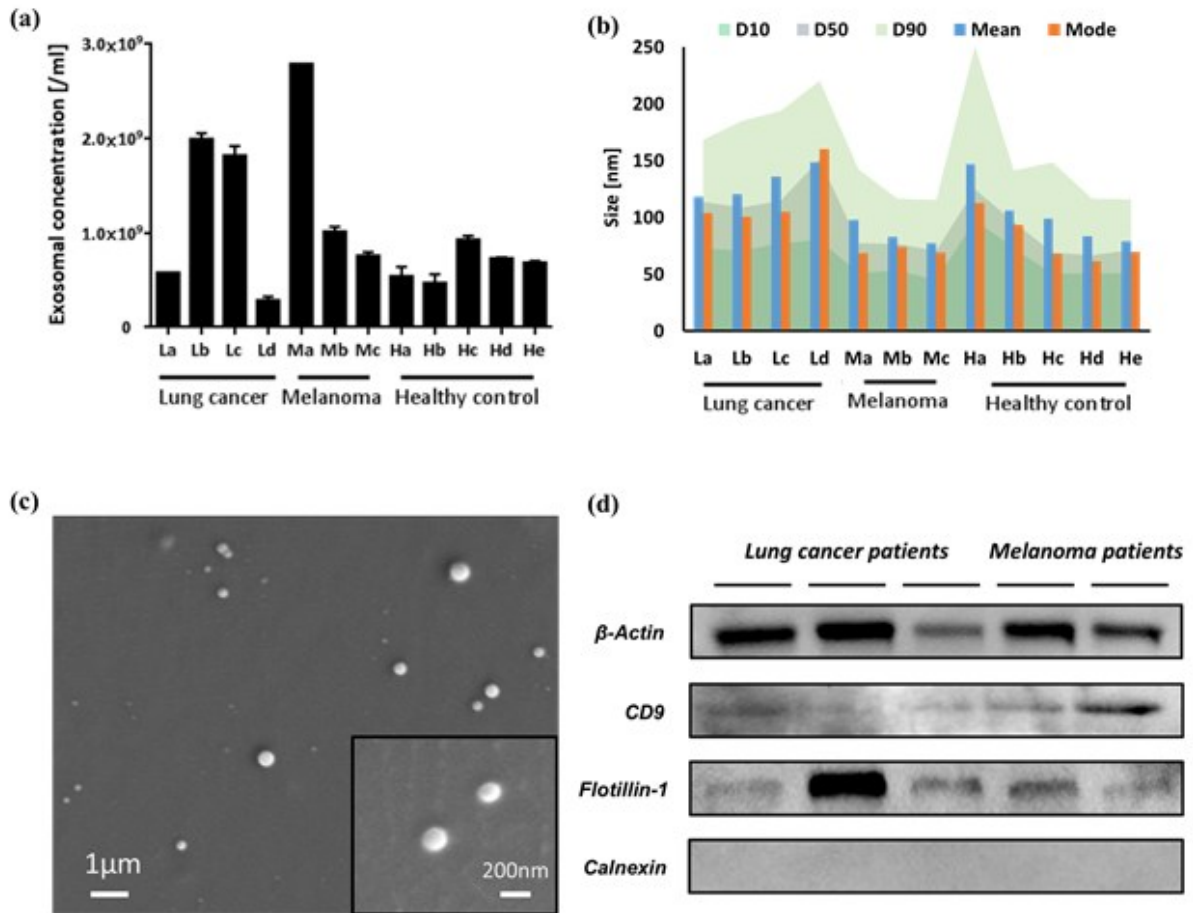
Figure 8. Isolation of exosomes from clinical samples from cancer patients and healthy donors. **a)** vesicle size distribution regarding mean, mode, and *D*-values (*D*10, *D*50, and *D*90) after release. **b)** exosome concentration after ^{new}ExoChip-based exosome recovery. **c)** SEM image of isolated exosome and the magnified view of the exosome from a melanoma patient. **d)** a representative western blot analysis of the protein isolated from ^{new}ExoChip and characterized for exosomal markers and intracellular protein marker in five different cancer patients' plasma samples.
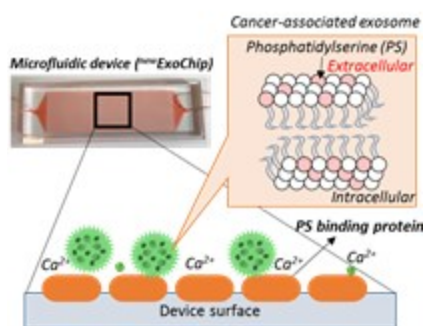
Table of Contents

Keyword: **Exosome isolation**

Yoon-Tae Kang, Emma Purcell, Colin Palacios-Rolston, Ting-Wen Lo, Nithya Ramnath, Shruti Jolly and Sunitha Nagrath[*]

Isolation and profiling of circulating tumor-associated exosomes using extracellular vesicular lipid-protein binding affinity based Microfluidic device

On-chip **exosome isolation** using immunoaffinity capture has improved recovery from small sample volumes compared to ultracentrifugation. However, tetraspanins are not specific to cancer exosomes and some cancers secrete exosomes with low expression of tetraspanins. Here, a microfluidic-device conjugated with proteins against phosphatidylserine (PS), shown to be expressed on the outer surface of cancer-associated exosome, were used to isolate cancer-associated exosomes.